Theor Chem Acc (2011) 128:683–694
DOI 10.1007/s00214-010-0798-3

REGULAR ARTICLE

DFT and kinetics study of O/O_2 mixtures reacting over a graphite (0001) basal surface

Víctor Morón · Pablo Gamallo · Ramón Sayós

Received: 28 June 2010 / Accepted: 13 August 2010 / Published online: 28 August 2010

Abstract Spin-polarized density functional calculations were used to investigate the interaction of atomic and molecular oxygen on the basal graphite surface at several atomic coverages. Two carbon layers were enough to represent the graphite surface. Oxygen atoms bind mainly over C–C bridge sites forming an epoxide-like structure with a two carbon puckering and with adsorption energies in the 0.95–1.28 eV range, depending on the atomic coverage. Molecular oxygen only shows a very weak physisorption. Atomic adsorption and diffusion along with atomic recombination via Eley–Rideal and Langmuir–Hinshelwood mechanisms were studied. All surfaces processes were activated with energy barriers that decreased for lower atomic coverages. Relaxation effects were non-negligible. A microkinetic model with six elementary surface processes was proposed to see the overall behaviour of several initial O/O_2 mixtures flowing over a graphite surface at 300–1,000 K. Thermal rate constants were derived from Density Functional Theory data and standard Transition State Theory. A very low steady-state atomic coverage ($\theta_O < 0.5\%$) was predicted, and also very low atomic recombination coefficients were observed ($\gamma_O < 5 \times 10^{-4}$). The Eley–Rideal together with the adsorption and desorption processes was much more important than the Langmuir–Hinshelwood reaction.

Published as part of the special issue celebrating theoretical and computational chemistry in Spain.

V. Morón · P. Gamallo · R. Sayós (✉)
Departament de Química Física and Institut de Química Teòrica i Computacional (IQTC-UB), Universitat de Barcelona, C. Martí i Franquès 1, 08028 Barcelona, Spain
e-mail: r.sayos@ub.edu

Keywords Adsorption · Diffusion · Atomic recombination · Oxygen · Graphite · Microkinetic model

1 Introduction

Carbon-based materials have received considerable attention for their use in spacecraft components (e.g., reinforced C was used as a thermal protection system (TPS) in the nose of Space Shuttle) due to their light weight and high strength. In the low Earth orbits (LEO), 160–2,000 km above Earth's surface, atomic oxygen is one of the main present species and can collide with the spacecraft surface at very high translational energies (i.e., about 4.5 ± 1.0 eV due to the orbital velocity of around 7.5 km/s) producing an important etching, hence degrading any C-based TPS [1]. Moreover, during hypersonic re-entry flights into Earth's atmosphere (e.g., Space Shuttle) not only atomic oxygen but also molecular oxygen processes can be relevant to understand properly the huge heat transfer and the TPS behaviour under these extreme conditions [2]. Therefore, a good understanding of all elementary processes involving atomic and molecular oxygen with carbon-based materials is essential for space technology. Thus, in principle, several heterogeneous processes could compete: (a) O adsorption, (b) O_2 dissociative or non-dissociative adsorption, (c) O recombination via an Eley–Rideal (ER) mechanism (i.e., $O_{(g)} + O_{ad} \rightarrow O_{2\ (g)}$), (d) O recombination via a Langmuir–Hinshelwood (LH) mechanism (i.e., $O_{ad} + O_{ad} \rightarrow O_{2\ (g)}$) and (e) C etching producing CO or CO_2, where ad labels adsorbed species and g gas species. Another less important elementary processes could also be added.

There are abundant theoretical studies about the interaction of atomic and molecular oxygen with graphite [3–7],

graphene [8, 9] and carbon nanotubes [4, 10, 11] covering different aspects but without giving a global approach about the O/O_2 reactivity over these carbon surfaces. They are mainly concerned with adsorption studies over several type of surfaces (e.g., basal, zig-zag, armchair, …) for different coverages. Thus, there was shown that atomic oxygen becomes mainly chemically adsorbed on a bridge position between two adjacent C atoms of graphite or graphene, forming an epoxy group, with adsorption energies in the range of 1.5–3.2 eV for a basal graphite surface depending on the oxygen coverages and the level of the calculations [3–6]. The molecular oxygen seems to be only physically adsorbed on basal graphite surfaces with low adsorption energies of about 0.12 ± 0.01 eV at 1 ML coverage as it has been shown using thermal desorption spectroscopy on highly oriented pyrolytic graphite (HOPG) [12]. Common density functional theory (DFT) studies are not accurate enough to provide reliable adsorption energies for O_2 over graphite [3, 4, 7], due to the importance of the missing van der Waals (vdW) contributions. Nevertheless, a suitable vdW treatment could be done for instance by adding pairwise interatomic C_6R^{-6} terms, where C_6 coefficients can be derived from ground-state electron density for molecules and solids [13]. The inclusion of vdW interactions reproduces quite well the O_2 physisorption over graphite [14, 15]. The interaction of O_2 with defective edge sites on graphite surfaces presents high adsorption energies (2.6–6.2 eV [7]) in a similar way as for atomic oxygen (4.5–5.7 eV [6]). Moreover, molecular oxygen reactively adsorbs on edge graphite surfaces at 300 °C and 1 atm pressure (the perfect basal surface is hardly active [16]), being the energy barrier for O_2 dissociation larger and for CO formation lower when the oxygen surface coverage diminishes [17].

Up to our knowledge, there are no theoretical studies about the ER and LH atomic reactions or on the atomic diffusion over graphite surfaces. Characterization of these reaction pathways is missing, and it is very important from a kinetic point of view. Only very recently, the migration (diffusion) barrier for O on a graphene sheet has been investigated [8], indicating an energy barrier of 0.58 eV at a coverage of 16.7%, which would imply a noticeable mobility of isolated adsorbed atoms.

Apart from the mentioned experimental studies about O_2 adsorption/desorption on graphite, there are as well a large number of experimental works concerned mainly with the interaction of hyperthermal atomic oxygen on HOPG surfaces, to understand the erosion and degradation of these surfaces under large collision energies [1, 18, 19], forming CO and CO_2 gas species.

In this work, we study the main elementary processes involving O and O_2 over an initially clean graphite basal surface (0001) at the same DFT level, characterizing not only the minima but also the transition states (TS) for the different processes at several oxygen coverages. These data are used in a proposed microkinetic model based on calculated thermal rate constants derived from Transition State Theory, which allows a kinetic study for different temperatures and total and partial pressures (i.e., several O/O_2 mixtures). We also determine the atomic oxygen recombination coefficient $\gamma_O(T, P)$ ($0 \leq \gamma_O \leq 1$), which is defined as the total probability of atomic oxygen recombination per atomic oxygen surface collision; γ_O values are necessary in standard computer fluid dynamics (CFD) simulations [2] of hypersonic flights aiming to evaluate their aerodynamic heating.

2 Computational details

The periodic DFT calculations presented in the current work have been carried out using the Vienna ab initio simulation package (VASP) code [20–23], which uses plane wave basis set. The calculations are mainly based on the generalized gradient approximation (GGA) functional revised Perdew-Burke-Ernzerhof functional (RPBE) [24]. However, some initial tests were also done with Perdew-Burke-Ernzerhof (PBE) [25, 26] and Perdew–Wang 91 (PW91) [27, 28] functionals. The projector-augmented-wave (PAW) technique within the frozen core approximation has been used to describe the electron-core interaction [29, 30]. An energy cut-off of 550 eV has been used in the plane-wave expansion after several tests to confirm the energy convergence of the calculations. Integration over the Brillouin zone was performed by using a $14 \times 14 \times 1$, $11 \times 11 \times 1$ and $6 \times 6 \times 1$ *k*-point meshes by means of the Monkhorst–Pack method [31] for slab calculations using several supercells, 1×1, 2×2 and 3×3, respectively. For bulk calculations, a $14 \times 14 \times 4$ *k*-point mesh was used. The atomic positions were partially (e.g., for gas/rigid slab system) or fully relaxed by using a quasi-Newton algorithm until the energy decreased below 10^{-5} eV, which usually corresponded to forces lower than 10^{-2} eV/Å. The energy convergence in the electronic self-consistent cycles was maintained below 10^{-6} eV for all geometrical optimizations and vibrational frequency calculations. The vacuum used in the slab model was around 15 Å, which was large enough to prevent significant interactions between periodic images.

Due to the important role that spin plays in both atomic and molecular oxygen (i.e., triplet in their ground states), all calculations were spin-polarized.

Several adsorption sites have been studied for O and O_2 species (see next section for details). Moreover, we have calculated minimum energy reaction paths (MERP) for the above-mentioned elemental processes (e.g., ER reaction,

atomic diffusion,.) by means of the climbing Nudged Elastic Band method (NEB) [32, 33] or using more simple reaction coordinates (e.g., Z_O distance over a C–C bridge site). Once determined the optimal geometry for each stationary point, we have calculated the Hessian matrix and its corresponding harmonic vibrational frequencies (v_i) to verify if they were true minima or transition states. We have also checked the connection among these stationary points. In general, we have fixed the optimized slab geometry, although some calculations with full or partial slab relaxation were also performed. Energy barriers ($\Delta E^{\neq}$) for the elementary processes were mostly computed using the corresponding supermolecule energy, calculated for reactants far enough to give a converged asymptotic energy.

The adsorption energy (E_{ad}) was calculated according to Eq. 1,

$$E_{ad} = (E_X + E_{slab}) - E_{X/slab} \quad (1)$$

where E_X is the energy of an isolated O or O_2 species at their electronic ground state, E_{slab} is the energy for the relaxed clean slab ($E_X + E_{slab}$ calculated as E_{X+slab}), and $E_{X/slab}$ is the energy of the adsorbed-slab system. Therefore, a positive adsorption energy means that this site is more stable than the X + slab asymptote; on the contrary, a negative adsorption energy corresponds to a less stable one.

The atomic energy (i.e., −2.41648 eV) was calculated with the oxygen atom inside a large broken symmetry box (e.g., 16 × 18x17 Å^3). The optimized O_2 molecule corresponds to an energy of −10.498232 eV, giving place to a dissociation energy (D_e) of 5.66 eV, an equilibrium distance (R_e) of 1.2348 Å and a vibrational frequency (v_e) of 1,556.0 cm^{-1}, which compare reasonably well with the experimental values 5.21 eV, 1.2075 Å and 1,580.2 cm^{-1} [34], respectively, in spite of the well-known problems to describe the dissociation energy of this open shell molecule, which depends both on the functionals and on the pseudopotentials used [24].

Thermal rate constants are derived from standard Transition State Theory formula, including reactants and transition state zero point vibrational energies [35].

3 Results and discussion

3.1 Bulk graphite properties

Graphite is formed by a layered structure of six-member carbon rings, stacked in an ABAB sequence with a weak interlayer binding compared to the much stronger binding within the layers. The experimental [36] lattice parameters for graphite structure are reported in Table 1.

We have calculated the graphite lattice parameters using several functionals (PW91, PBE and RPBE). The value of optimum $a = b$ lattice parameter is similar and close to the experimental value [36], although the optimum c lattice parameter is overestimated in all cases. The usual fail of GGA approximation to predict the c-axis lattice parameter and the small interlayer binding energy is well known, along with the better LDA description of c (Table 1); the inclusion of empirical vdW interactions [37] on both GGA and LDA calculations produces as well good calculated interlayer binding energies. On the contrary, GGA gives much better cohesive energies, being the RPBE value (7.516 eV/atom) very close to the experimental value

Table 1 Calculated and experimental lattice parameters, interatomic distances, cohesive energy, isotropic bulk modulus and its pressure derivative for graphite compound

Method	$a = b$ (Å)	c (Å)	d_{C-C} (Å)	E_{coh} (eV/atom)[a]	B_{iso} (GPa)[a]	B'_{iso} [a]
PW91	2.465	7.698	1.423	7.856	275.4	4.04
PBE	2.467	7.816	1.425	7.847	277.4	3.69
RPBE	2.467	8.022	1.425	7.516	270.3	4.29
LDA/CA[b]	2.441	6.64	–	8.903	–	–
GGA/PW91[b]	2.461	~9.0	–	7.865	–	–
Experiment	2.456[c]	6.696[c]	1.418[c]	7.371 ± 0.005[d]	318 ± 11 (0 K)[e] 286 ± 11 (300 K)[e]	13.6 (295 K)[f]

[a] E_{coh}, B_{iso} and B'_{iso} were calculated using the experimental c lattice value

[b] LDA/Ceperley–Alder and GGA/Perdew–Wang 91 previous calculations with ultrasoft pseudopotentials [37]

[c] Experimental values [36]

[d] Experimental value [38] derived from $\Delta_f H^o(0\ K)$ for the process: C(graphite) → C(g,ideal)

[e] Experimental values [40, 41] obtained from elastic constants (C_{ij}) through the formula

$B_{iso} = \frac{2}{9}(C_{11} + C_{12}) + \frac{4}{9}C_{13} + \frac{1}{9}C_{33}$, [42]

[f] Experimental value [40] obtained from the pressure derivative of the previous equation

(7.371 eV/atom). The cohesive energy was calculated from the equation,

$$E_{\mathrm{coh}} = \frac{1}{N_{\mathrm{C}}}\left(N_{\mathrm{C}}E_{C(g)} - E_{\mathrm{bulk(eq.)}}\right) \quad (2)$$

where N_{C} is the number of C atoms in the cell, $E_{\mathrm{C(g)}}$ is the energy of C (triplet) atom, and $E_{\mathrm{bulk(eq.)}}$ is the energy corresponding to the equilibrium bulk structure with optimum a and experimental c lattice parameters.

Table 1 also presents the isotropic bulk modulus (B_{iso}) and its pressure derivative (B'_{iso}) obtained from volume changes with a constant c/a ratio, with several c values close to the experimental lattice parameter. B_{iso} and B'_{iso} are derived by means of a fit to the calculated pressure–volume data using the third-order Birch-Murnaghan equation of state [39]. The calculated B_{iso} values are very similar and in good agreement with experimental ones, which were derived from the elastic constants of pyrolytic graphite [40, 41]. The correct calculation of the usual bulk modulus (B_{o}) for highly anisotropic materials implies the use of an uniaxial compression [43] instead of an uniform compression, which could produce values an order of magnitude larger than the experimental ones. Hence, the poor description of the c lattice parameter does not allow a proper calculation of B_{o} with the present DFT/GGA calculations.

The calculated B'_{iso} are much lower than the experimental values estimated from the initial slopes of elastic constants with pressure at atmospheric pressure and 295 K [40] as shown in Table 1.

In general, we conclude that GGA/RPBE calculations give a reasonable good description of bulk graphite properties, although it is necessary to use the experimental c lattice parameter. This will not be a problem for the reliability of the atom or molecule-slab calculations of the next section as it has been also assumed in similar previous studies [6].

3.2 Adsorption and diffusion of oxygen

We have studied the adsorption of atomic oxygen on the basal (0001) graphite surface, with a slab formed by one or two carbon layers. The results are almost identical regardless of the number of layers of the slab model, possibly due to the very weak interlayer interaction. This fact was also verified in previous O and K adsorption studies over graphite [3] by using 1, 2 or 3 layers. Hence another similar O/graphite studies have simulated the graphite as a single sheet of C atoms [4].

Three high-symmetry different sites have been mainly considered (Fig. 1): on top of a surface C atom, which is either above another C atom (T1) or above an hexagon hollow (T2) from the adjacent plane, and over a bridge

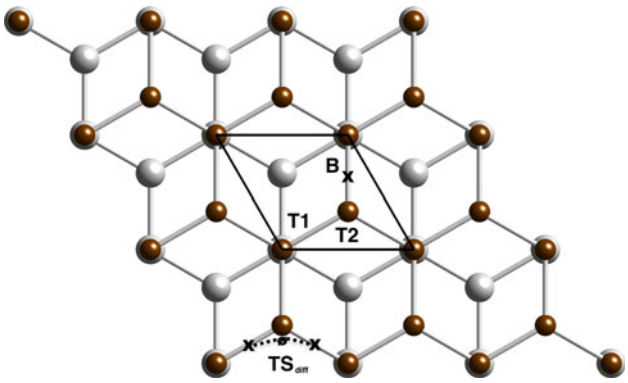

Fig. 1 *Top* view of the graphite (0001) slab two-layer model with the different adsorption sites: bridge (B), on top a C with also a C below (T1) and on top a C without a C below (T2). The atoms of the second layer are plotted a bit larger and with light colour to be distinguished from first layer atoms. The transition state for O diffusion between two bridge adsorption sites is also shown. The *solid line* shows the surface 1 × 1 unit cell

between the two nearest-neighbour carbon atoms (B). We checked also that the hollow of the hexagonal ring of the first layer did not present any significant adsorption in agreement with previous studies [5, 6]. The atomic coverage effect has been studied considering the adsorption of one O atom over three different unit cells: 1 × 1, 2 × 2 and 3 × 3, namely 50, 12.5 and 5.5% with respect to the C atoms (i.e., T1 and T2 sites). These coverages would be doubled taking into account only the most stable adsorption sites (i.e., true minima), which correspond to the bridges (i.e., B sites); when an O is over a bridge site the closest free bridges become unavailable for another O adsorption because every C atom can make only four bonds. We will indicate this coverage throughout the text giving both values (i.e., % with respect to C or top sites/% with respect to bridge sites).

Table 2 presents the results for the atomic adsorption on T1, T2 and B sites for several oxygen coverages for a two-layer rigid slab. There are negligible differences with respect to the very small adsorption energies or the O–C distances for T1 and T2 sites. The bridge site is the most stable one for all coverages. The analysis of its harmonic vibrational frequencies shown in Table 1 reveals that it is a true minimum (i.e., all positive frequencies), and this is more stable for high O coverages, where O images are much closer (e.g., the minimum $d_{\mathrm{OO}} = a = 2.467$ Å for 50% coverage) and can introduce an extra stabilization, in a similar way as was observed for O/graphene [8].

In all calculations, we observe that the singlet state is the most stable state for all sites in agreement with previous studies for O/graphite [4–6]. In general, the present results are quite similar to the extensive study of Incze et al. [5, 6] by using GGA/PW91 with ultrasoft Vanderbilt type pseudopotentials, although they obtained larger adsorption

Table 2 Calculated properties for O adsorption over a basal (0001) graphite surface, without slab relaxation

Coverage (%)[a]	Site[b]	E_{ad} (eV)	z_O (Å)	d_{O-C} (Å)	ν_i (cm^{-1})[c]	
					⊥	∥
50/100	T1	−0.816	1.544	1.544	574.5	367.2i 374.2i
	T2	−0.811	1.509	1.509	571.0	407.6i 410.5i
	B	0.881	1.251	1.440	822.6	610.6 379.7
12.5/25	T1	0.281	1.556	1.556	542.7	89.0i 95.1i
	T2	0.308	1.554	1.554	583.2	196.1i 201.2i
	B	0.660	1.385	1.557	548.7	325.8 315.2
5.5/11.1	T1	0.0215	1.589	1.589	489.7	142.0 133.1
	T2	0.0673	1.584	1.584	526.8	151.7i 170.5i
	B	0.541	1.384	1.557	538.3	389.4 350.0

The slab geometry (two C layers) is fixed at its optimum geometry (d_{C-C} = 1.425 Å) derived in absence of O but with the interlayer distance (d_{12}) fixed to its experimental value (3.347 Å)

[a] The coverage is calculated with respect to the top sites (O/C %) or the bridge sites (O/bridge%) to facilitate the comparison with previous studies

[b] In T1 and T2 sites, only the z_O variable is optimized

[c] Harmonic vibrational frequencies of the atomic adsorbate with respect to the rigid substrate. The first one corresponds to a perpendicular vibration and the other to parallel vibrations to the graphite surface

energies for bridge site (1.89 and 1.73 eV for 50 and 5.5% O/C coverages, respectively), within the rigid slab approximation.

T1 and T2 stationary points mainly present two imaginary frequencies, which seem to connect with the adsorption bridge minimum and with a diffusion transition state (see below for more details), although the slab relaxation can affect as well the character of these frequencies (e.g., reducing to one imaginary value for T1 site at 12.5/25% coverage).

Table 3 summarizes the effect of slab relaxation in the bridge minimum for several O coverages. This geometry relaxation corresponds to a stretching of C–C bond along with a reduction of both C–O bonds, with also a puckering of the two carbon atoms beneath the adatom. This behaviour is in good agreement with a similar DFT study by means of GGA/PW91 with ultrasoft pseudopotentials [4], which shows d_{O-C} = 1.472 Å and d_{C-C} = 1.500 Å, compared to the graphite d_{C-C} = 1.420 Å for a 5.5/11.1% of coverage. However, a larger adsorption energy (1.91 eV) was calculated in that work. We observe as well that the slab relaxation implies that the adsorption energy tends to be larger for low O coverages (Table 3), conversely to the behaviour found for rigid slab (Table 2).

The formation of this epoxide-like (COC) ring structure on bridge sites has been observed in theoretical and experimental studies on graphene [9] and graphite [44–46] oxides. Thus, for symmetrical graphene epoxide [9], the calculated values, d_{O-C} = 1.42–1.44 Å and d_{C-C} = 1.49–1.50 Å (d_{C-C} = 1.41 for clean graphite) at high coverages show a similar trend as in the present work for oxygen over graphite. The epoxide groups enhance the wrinkling of carbon sheets (i.e., z_C = 0.25–0.27 Å, Table 3) in agreement with previous Monte Carlo studies on graphite oxide ($\langle z_C \rangle$= 0.33 ± 0.04 Å [46]). The oxidation of graphite increases also its interplanar spacing from 3.39 Å to 6.91–6.96 Å due to the expansion of the layer planes originated by the accommodation of various oxygen species, according to experiments [44, 45] and Monte Carlo simulations [46]. In the present study, with only O and O_2 gas species, we believe that sub-surface processes (e.g., O or O_2 penetration) will be negligible. For instance, in the centre of the hexagonal hollow, where O could seemingly enter into the sub-surface, the energy is very repulsive for O approach (e.g., for Z_O = 1.91, 1.52 and 1.12 Å the energy is 0.43, 1.51 and 4.52 eV with respect to O + slab asymptote, respectively). Another possibility for O penetration into the slab could be through the same O bridge adsorption, although this would imply the breaking of the underlying C–C bond, but this process seems to be infrequent as it has been shown in Monte Carlo simulations on graphite oxidation [46], where the use

Table 3 Calculated properties for O adsorption over a bridge site of a (0001) graphite surface, with some slab relaxation

Coverage (%)	E_{ad} (eV)	z_O (Å)[a]	z_C (Å)[a]	d_{O-C} (Å)	d_{C-C} (Å)	ν_i (cm^{-1})[c]	
						⊥	∥
50/100	0.945	1.254	–[b]	1.437	1.432	830.7	617.8 400.7
12.5/25	1.283	1.532	0.246	1.482	1.472	652.4	411.3 337.2
5.5/11.1	1.255	1.547	0.267	1.478	1.479	655.2	438.1 337.0

The carbon atoms directly bound to oxygen adatom on *B* site are allowed to relax in all directions

[a] z = 0 at the first layer formed by the C atoms without including the carbons underneath the O, which are at d_{C-C} separation

[b] For the highest coverage (50/100%), the C relaxation implies that all the first layer is shifted upwards (i.e., d_{12} increases to 3.957 Å). For another coverages, d_{12} is kept fixed to its experimental value (3.347 Å)

[c] Harmonic vibrational frequencies of the atomic adsorbate with respect to the rigid substrate. The first one corresponds to a perpendicular vibration and the other to parallel vibrations to the graphite surface

of only one C layer and the additional presence of H could facilitate even more this occasional process in comparison with our 2 layer model with only pure oxygen.

We have also observed a slight interlayer (d_{12}) enlargement for O adsorption at the highest coverage (50/100%, Table 3), when slab was allowed to relax, but without O penetration into the slab. In fact, we have fixed the interlayer distance to its experimental value in almost all calculations due to the poor description of vdW interactions with the present DFT approach.

A Bader charge analysis of the epoxy group shows an important charge transfer between the C atoms of the surface and the adsorbed oxygen (e.g., $q_O = -0.99$, $q_C = +0.41$, $+0.58$ at 50/100%). This arrangement of negatively charged oxygen could avoid the nucleophilic attack on C atoms, explaining the relative chemical stability of the epoxide groups in graphite oxides, as it was earlier suggested [44].

Table 4 summarizes the properties of transition states for O adsorption and diffusion processes over the basal (0001) graphite surface at several coverages for rigid slab approximation. Adsorption process is clearly activated as it was also demonstrated for atomic hydrogen over graphene ($\Delta E^{\neq} \sim 0.14$ eV at low coverages [47]) or graphite ($\Delta E^{\neq} = 0.23$ eV at 12.5/25% coverage [48]). The main difference is that H is mainly adsorbed on top carbons while O prefers the bridge sites. In spite of H and O have different electronic properties, their open shell nature could justify the rather similar behaviour when reacting over the same substrate.

The energy barrier is larger for high O coverages, although slab relaxation tends to decrease this barrier as we have observed for 12.5/25% coverage calculations (Table 4). Usually, more exothermic reactions (i.e., atomic adsorption with slab relaxation) show lower energy barriers (i.e., early TS) in agreement with Hammond's Postulate. The slab relaxation modifies mainly the z of both C atoms below the O adatom, but the O–C distances are almost unchanged (Table 4).

The analysis of the imaginary frequency in this transition state confirms that principally the perpendicular movement of oxygen with respect to the surface (i.e., z_O coordinate) corresponds to the adsorption process. This TS has mainly a triplet character due its proximity to the O gas asymptote.

The diffusion of one absorbed O over a bridge to its closest bridge is also an activated process that follows a path roughly shown in Fig. 2, with a TS mainly with a singlet character as in the adsorption minimum. The imaginary frequency involves mostly a parallel movement to the surface as could be expected for this process. The corresponding energy barrier decreases significantly when the coverage is reduced, likewise as for the adsorption process. However, the slab relaxation increases considerably this

Table 4 Calculated properties of the transition states for O adsorption and diffusion processes over the basal (0001) graphite surface

Process and coverage[a]	$\Delta E^{\neq}$ (eV)[b]	z_O (Å)[c]	d_{O-C} (Å)[c]	ν_i (cm^{-1})[d]	
				⊥	∥
$O_g + s \rightarrow O_{ad}$ *(adsorption)*					
50/100%	0.67 (0.69)	1.755	1.878, 1.910	535.4i	220.2 123.4
12.5/25%	0.31 (0.32)	1.874	1.940, 2.090	734.1i	103.8 47.5
	0.19 (0.13)[e]	2.060	1.863, 1.918	112.1i	266.7 171.1
5.5/11.0%	0.28[f]	1.848	1.981, 1.981	–	
$O_{ad} + s' \rightarrow O_{ad'} + s$ *(diffusion)*					
50/100%	1.43 (1.49)	1.425	1.955	675.1	611.7i 306.4
12.5/25%	0.38 (0.42)	1.553	1.555	549.7	188.6i 113.0
	0.73 (0.70)[e]	1.718	1.421	709.6	157.3 101.7i
5.5/11.1%	0.47 (0.51)	1.585	1.588	519.9	169.8 97.8i

The slab geometry (two C layers) is fixed at its optimum geometry ($d_{C-C} = 1.425$ Å) derived in absence of O but with the interlayer distance (d_{12}) fixed to its experimental value (3.347 Å)

[a] s or s′ correspond to C–C bridge sites

[b] Energy barriers with respect to reactants (including zero point energy between parentheses)

[c] The transition state for adsorption is practically over the C–C bridge site and for diffusion is between two non-adjacent C atoms (see Fig. 1)

[d] Harmonic vibrational frequencies of the atomic adsorbate with respect to the rigid substrate

[e] In this case, the carbon atoms directly bound to oxygen adatom are allowed to relax in all directions (i.e., $z_C = 0.314$ and 0.297 Å for adsorption and diffusion TSs, respectively)

[f] This TS was derived approximately from the crossing between the singlet and triplet curves

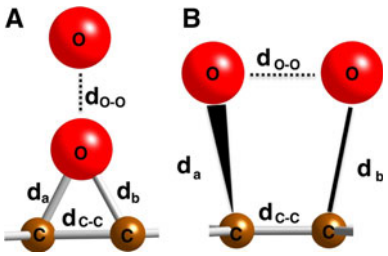

Fig. 2 Geometries corresponding to transition states for: **a** ER reaction and **b** LH reaction, labelling the different interatomic distances

energy barrier from 0.38 to 0.73 eV at 12.5/25% (Table 4) as could be expected because the adsorption energy of adatom changed from 0.66 to 1.28 eV due to C relaxation in z direction. Therefore, the adatom should diffuse quickly over the graphite surface only at high temperatures, which is also in agreement with previous values derived for O over graphite ($\Delta E^{\neq} \geq 0.36$ eV at 3.12% [3]) or graphene ($\Delta E^{\neq} = 0.58$ eV at 16.7% [8]).

We have also studied with the present DFT approach the adsorption of molecular oxygen on the basal surface of graphite. Thus, perpendicular and parallel initial configurations with its centre of mass over the different adsorption sites (Fig. 1) were considered, optimizing all degrees of freedom including also the slab relaxation by using a 2 × 2 unit cell. There were found very low adsorption energies ($E_{ad} \leq 0.01$ eV) at long distances of the centre of mass from the surface ($z_{com} = 3.70$–3.75 Å) with O–O bond distances of 1.238 Å, slightly larger compared to the free molecule bond distance of 1.235 Å. These results are quite similar to previous studies that used either a cluster ($E_{ad} = 0.011$ eV, $z_{com} = 4.212$ Å, $d_{OO} = 1.167$ Å compared with 1.166 Å in O_2(g) [7]) or a slab model ($E_{ad} = 0.039$ eV, $z_{com} = 3.362$ Å, $d_{OO} = 1.238$ Å compared with 1.237 Å in O_2(g) [4]) over graphite, which also showed that triplet state was more stable than the singlet one. The quality of the DFT spin description of this system would not possibly explain these energy differences because we observed as well a clear and reasonable spin polarization involving mostly the gas and some of the first layer slab atoms in another very similar studies (e.g., O and N over β-cristobalite [49] or O over α-alumina [50]). We think that those could be rather originated by the DFT limitations to describe the vdW interactions, whose importance has also been postulated in some previous experimental and theoretical studies for O_2 with carbon SWNT bundles or graphite [14, 15], as it was explained in the introduction. Therefore, a better DFT description should be necessary to account for the small experimental physisorption energy (0.12 ± 0.01 eV at 1 ML coverage [12]).

3.3 Recombination reactions of atomic oxygen

We have calculated MERPs for ER and LH processes by means of the climbing NEB method, using at least 6 images. For instance, for ER reaction, the first image was an O adatom over a bridge along with the $O_{(g)}$ above it but well separated from the surface, and the final image was an $O_{2(g)}$ in a perpendicular configuration far from to the surface. We checked that the final stationary points had the lowest energies and that they properly correspond to ER or LH processes, being therefore independent of the MERPs. Moreover, as we are preparing the construction of two interpolated PESs for O/graphite and O_2/graphite or O/O-graphite dynamical studies, we have also calculated grids of points at different geometries over the unit cell, whose energies are in complete agreement with the proposed stationary points of the present work.

We have found that the atomic recombination processes (i.e., ER and LH reactions) over the basal (0001) graphite surface are activated processes although their energy barriers considerably decrease with coverage increment, as can be seen in Table 5. The ER transition state corresponds to a perpendicular O–O orientation over the bridge site (Fig. 2), being the imaginary frequency also a perpendicular movement that gives place to $O_{2(g)}$. Contrarily, the LH transition state presents a parallel configuration (Fig. 2) with a similar O–O distance as for ER TS (e.g., for a (2 × 2) unit cell); in this case, the imaginary frequency has a mixture of both parallel and perpendicular movements, as could be expected. There is not experimental information to compare with these energy barriers. However, a similar DFT study with H over graphite (0001) surface for a 12.5/25% coverage shows that at this low coverage the ER energy barrier would be equally very low (≤0.05 eV), as could be observed from cross-sections vs. incident energy plot of quantum scattering calculations [48]). However, the authors assumed a puckering of the C atom below the adsorbed H on top ($z = 0.36$ Å), which possibly reduces more this ER energy barrier. Conversely, the relaxation of the slab in the present study could increase this energy barrier for O as occurred for the diffusion process (Table 4), because O adatom tends to become more stable (Table 3) after slab relaxation. This effect could also be expected for LH reaction, although the slab relaxation effect should be checked with additional calculations.

The LH reaction should be much less important than ER (or hot atom) reaction as can be concluded from the large differences in their energy barriers as will be confirmed in the next section. This fact has also been previously found out for these O recombination reactions over β-cristobalite [51].

Table 5 Calculated properties of the transition states for Eley–Rideal (ER) and Langmuir–Hinshelwood (LH) processes involving O atoms over the basal (0001) graphite surface

Process and coverage[a]	$\Delta E^{\neq}$ (eV)[b]	z_O (Å)[c]	d_{O-C} (Å) d_a, d_b^c	d_{O-O} (Å)	ν_i (cm^{-1})[d]	
					⊥	∥
$O_g + O_{ad} \rightarrow O_{2(g)} + s$ *(ER reaction)*						
50/100%	1.11 (1.06)	1.525, 3.235	1.685, 1.682	1.711	962.4i 246.7	339.7 152.8 124.2 63.5
12.5/25%	0.10 (0.076)	1.499, 3.492	1.647, 1.672	2.024	527.9i 209.5	301.8 268.4 87.7i 33.9
$O_{ad} + O_{ad} \rightarrow O_{2(g)} + 2$ s *(LH reaction)*						
25/50%	1.91 (1.87)	1.569, 1.570	1.609, 1.610	1.736	611.6i 496.8	397.4 330.0 256.2 196.0
11.1/22.2%	1.28[e]	1.600, 1.600	1.625, 1.622	1.774	–	

The slab geometry (two C layers) is fixed at its optimum geometry ($d_{C-C} = 1.425$ Å) derived in absence of O but with the interlayer distance (d_{12}) fixed to its experimental value (3.347 Å)

[a] s or s′ corresponds to C–C bridge sites. For LH reaction, coverages are necessarily doubled with respect to ER or adsorption processes when using the same unit cell

[b] Energy barriers with respect to reactants (including zero point energy between parentheses)

[c] The transition state geometries for ER and LH reactions are depicted in Fig. 2. <OCCO dihedral is 24.7° at 25/50% and 16.8° at 11.1/22.2% for LH TS

[d] Harmonic vibrational frequencies of the atomic adsorbate with respect to the rigid substrate. Approximately, the two first correspond to perpendicular and the other to parallel vibrations with respect to the graphite surface for the ER reaction. In the case of LH reaction the imaginary frequency shows as mixture of parallel and perpendicular movements

[e] This TS was derived approximately from some grids of points

3.4 A microkinetic model for O/O_2 mixtures over graphite

We propose a first microkinetic model to estimate the overall effect of all studied heterogeneous processes involving different O/O_2 mixtures over a graphite (0001) surface. Six surface elementary processes are included:

Chemisorption (k_1) and desorption (k_{-1}) of atoms:

$$O_{(g)} + s \underset{k_{-1}}{\overset{k_1}{\longleftrightarrow}} O_{ad} \tag{3}$$

Langmuir–Hinshelwood reaction (k_2) and dissociative molecular adsorption (k_{-2})

$$O_{ad} + O_{ad} \underset{k_{-2}}{\overset{k_2}{\longleftrightarrow}} O_{2(g)} + 2s \tag{4}$$

Eley–Rideal reaction (k_3) and another dissociative molecular adsorption channel (k_{-3})

$$O_{(g)} + O_{ad} \underset{k_{-3}}{\overset{k_3}{\longleftrightarrow}} O_{2(g)} + s \tag{5}$$

where s indicates a free site on the surface. Despite we list the elementary processes using direct and reverse notation, both type of processes can be produced simultaneously and almost independently (i.e., 2/−2 or 3/−3) for the several O/O_2 initial reactant's mixtures.

Non-dissociative molecular adsorption is not taken into account because the almost negligible above-mentioned O_2 physisorption. The O_2 dissociation can produce several final products (e.g., $O_{ad} + O_{ad}$, $O_{(g)} + O_{ad}$, …). The diffusion processes (e.g., $O_{ad} + s \rightarrow O_{ad}' + s'$, for instance between two bridge sites) will not have a global contribution to the final atomic coverage because its reverse process would cancel this ($r_{dis} = r_{-dif}$). However, diffusion could enhance the approach of two adatoms to adjacent bridges separated only with a C–C bond, which could improve the possible LH processes. Atomic diffusion should be included in kinetic Monte Carlo simulations, where non-uniform atomic coverages can occur but in our present and simple model with a uniform coverage assumption would not be necessary.

For each elementary step, the rate constant can be derived from the standard Transition State Theory [35] by the general equation

$$k(T) = \frac{k_B T}{h} \frac{q^{\neq}}{q_r} e^{-\Delta E_o^{\neq}/k_B T} \tag{6}$$

where k_B is the Boltzmann constant, T is the temperature (assuming that gas and surface temperatures are equal), h is the Planck constant, $q^{\neq}$ is the partition function of the transition state (lacking one degree of freedom), q_r is the partition function of reactants, and $\Delta E_o^{\neq}$ represents the energy barrier for the corresponding process including the zero point vibrational correction. In the case of LH and its reverse rate constants (i.e., $k_2(T)$ and $k_{-2}(T)$) also include the factor $1/[s]_o$, where $[s]_o$ is the initial surface density of free sites (i.e., 1.90×10^{19} bridge sites/m^2 for the graphite (0001) surface).

Certainly, during re-entry trajectories (e.g., Space Shuttle) there are several regimes depending on the altitude and the velocity of the vehicle: (a) chemical and thermal

equilibrium, (b) chemical non-equilibrium with thermal equilibrium and (c) chemical and thermal non-equilibrium inside the shock layer [2]. Near the surface (in the boundary layer), a lot of kinetic models assume thermal equilibrium with chemical non-equilibrium [52–54]. Therefore, a canonical ensemble approach seems to be suitable.

We have used the DFT data for slab rigid and low coverage calculations (i.e., 12.5/25% for one adatom processes or 11.1/22.2% for LH reaction) in order to derive the different thermal rate constants. Figure 3 shows the energetics of the different elementary steps and Fig. 4 the calculated TST rate constants within the 400–2,000 K range of temperature. It is evident that there are large differences in rate constants, which will have an important influence on the global kinetics of the system once the concentrations are included.

From the differential equation for adsorbed atomic oxygen, $(d[O_{ad}]/dt)$ can be developed the expression in terms of the atomic surface coverage (θ_O), which takes the form:

$$\frac{d\theta_O}{dt} = \theta_O^2\left(\frac{2}{3}k_{-2}[O_2][s]_0 - 2\frac{2}{3}k_2[s]_0\right) - \theta_O\left((k_1+k_3)[O] + 2\frac{2}{3}k_{-2}[O_2][s]_0 + k_{-3}[O_2] + k_{-1}\right) + \left(k_1[O] + \frac{2}{3}k_{-2}[O_2][s]_0 + k_{-3}[O_2]\right) \quad (7)$$

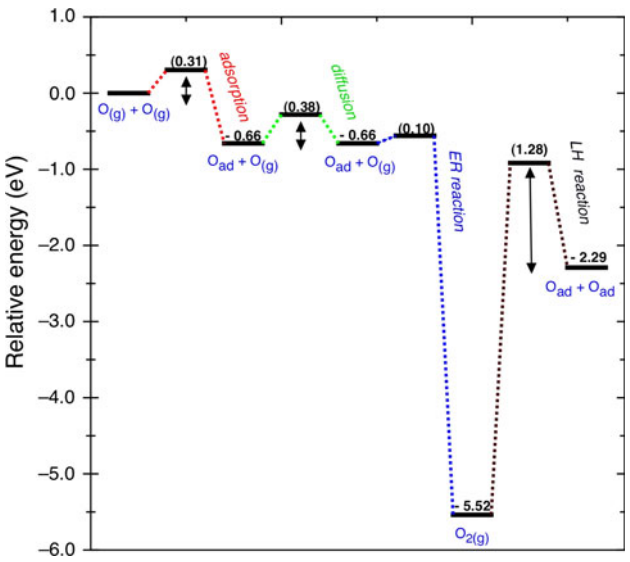

Fig. 3 Energy diagram for several O heterogeneous elementary processes over a graphite (0001) surface for a 12.5/25% coverage (11.1/22.2% for LH reaction). Values between parentheses give the energy barriers without ZPE with respect to the closest reactants. O_2 dissociation energy can change in approximately in ±0.1 eV due to a small size consistency problem in the asymptotes (i.e., $O(^3P) + O(^3P)$ + slab calculated as supermolecule or as fragments addition)

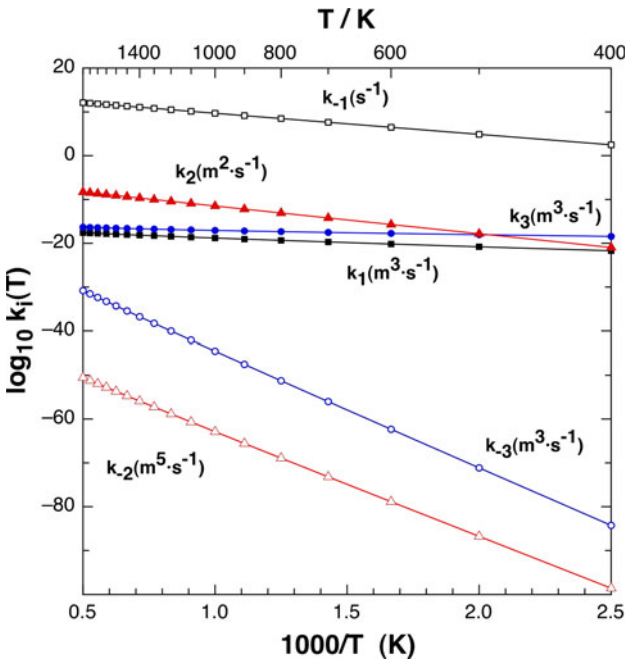

Fig. 4 Calculated TST thermal rate constants for the different heterogeneous processes involved in the proposed microkinetic model, based on DFT data for a 12.5/25% coverage (11.1/22.2% for LH reaction). Only k_i with same units (shown inside the plot) could be directly compared. Points are connected with a line to guide the view

where the 2/3 factor takes into account that only for LH reaction (or its reverse) two adatoms (or two free sites) not in adjacent bridges and separated only with a C–C bond are able to react (e.g., 4 from 6 possibilities in a 2 × 2 cell). The numerical integration of this differential equation for a constant flux of an O/O_2 mixture impinging over the surface allows to see the time evolution of θ_O.

The O and O_2 partial pressures are introduced through the [O] and $[O_2]$ concentrations (e.g., $[O] = P_O/RT$). In fact, we assume that these pressures are kept constant (i.e., $[O] \approx [O]_o$ and $[O_2] \approx [O_2]_o$) because the reactivity is very low and moreover in several experiments aiming to determine γ_O coefficients these initial concentrations seem to be constant [56, 57].

It is worth noting that a steady-state (ss) is reached rapidly for different initial conditions (i.e., P_O, P_{O2} and T) with a final low atomic coverage in all studied cases (Fig. 5). Figure 6 shows θ_O at several temperatures for two representative partial pressures although another combinations were also explored. Thus, very low values of a final steady-sate atomic surface coverage ($<10^{-3}$) are observed between 300 and 1,000 K for both mixtures, with larger values for the higher O partial pressure as could be predictable. This chemisorption of atomic oxygen on the (0001) graphite surface has been also revealed experimentally [16], with a low level of adsorption on the basal

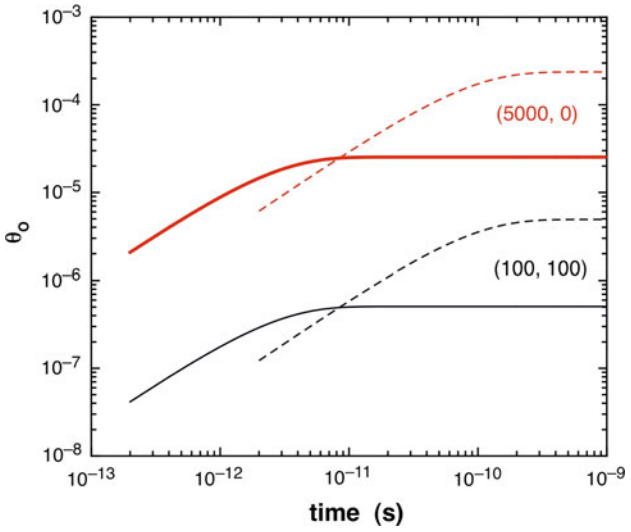

Fig. 5 Atomic surface coverage time evolution for two O/O_2 initial mixtures: (100, 100 Pa) and (5,000, 0 Pa) at 700 K (*dashed line*) and 900 K (*solid line*)

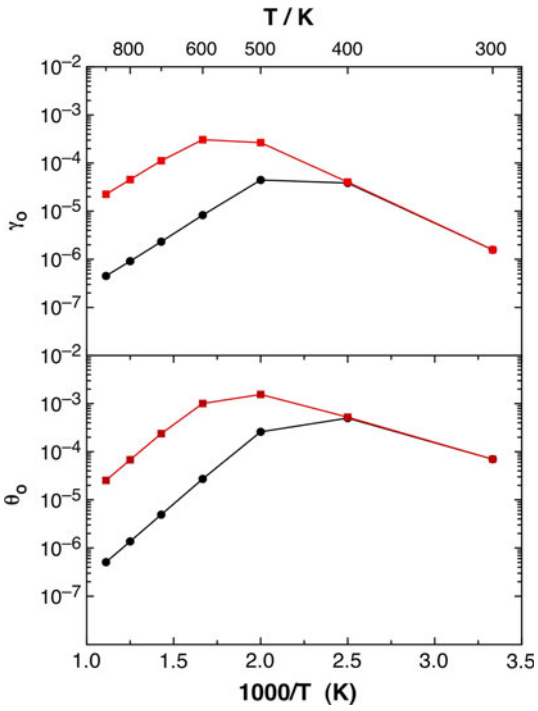

Fig. 6 Atomic surface coverage and γ_O coefficient in front the temperature for two O/O_2 initial mixtures: *circles* (100, 100 Pa) and *squares* (5,000, 0 Pa)

surface, mainly enhanced by the concentration of defect sites [17]. Moreover, these low final θ_O values support as well our use of DFT data for low coverage in the calculated rate constants.

The shape of θ_O as a function of the temperature shows a maximum at different temperatures (i.e., 400 and 500 K), which depends basically on the initial P_O value as could be expected because at high temperatures the desorption becomes the most important process.

We have also estimated the atomic oxygen recombination coefficient γ_O from the following equation,

$$\gamma_O = \frac{k_1[O]\left(1-\theta_{O(ss)}\right)[s]_0 + k_3[O]\theta_{O(ss)}[s]_0 - k_{-1}\theta_{O(ss)}[s]_0}{Z_O} \tag{8}$$

which includes only the process that directly involve atomic oxygen, namely adsorption, ER and desorption, once achieved the steady-state ($\theta_{O(ss)}$), and where Z_O is the number of O collisions per unit area and unit time with a planar surface (Hertz-Knudsen relation),

$$Z_O = [O]\sqrt{\frac{k_B T}{2\pi m_O}} \tag{9}$$

where m_O is the atomic oxygen mass.

The γ_O coefficient shown in Fig. 6 almost mimics the shape of the θ_O plot. An analysis of its three contributions establishes clearly that at low temperatures adsorption and ER reaction are the most important processes with similar contributions, while at high temperatures this occurs for adsorption and desorption processes although in this case their rates are counterbalanced (i.e., $r_1 = r_{-1}$), hence that γ_O finally decreases as a consequence of the lower $\theta_{O(ss)}$values. Although the final steady-state coverage depends as well on LH process (Eq. 7), in the present case its contribution is unimportant due to its low rate constants.

The comparison of the $\gamma_{O(T)}$ shape over graphite with respect to other materials (e.g., metals [55], alumina [56], silica [57], …) is similar but with much minor values. Moreover, the γ_O decline is produced at much lower temperatures for graphite, possibly as a consequence of its lower adsorption energies. The introduction of new rate constants based on DFT data with slab relaxation and/or higher coverages does not produce very important changes with respect to the present results as we have checked with some additional calculations, possibly because the very low γ_O values.

The presence of molecular oxygen (i.e., $P_{O2} \neq 0$) in the initial flux is negligible within the studied temperature range (300–1,000 K) for both γ_O and θ_O. This is supported by the large energy barriers (Fig. 3) associated with the two dissociative molecular processes (i.e., very small k_{-2} and k_{-3}) included into the microkinetic model.

The very low γ_O coefficients and the large melting point of graphite (4,800 ± 100 K at a pressure of 10–100 MPa [58]) could seemingly indicate that C-based materials would be a good proposal to be used as TPS for atmospheres containing oxygen. Nevertheless, the oxidative etching of graphite, forming $CO_{(g)}$ and also $CO_{2(g)}$, can

degrade this material and would prevent its use even at moderate temperatures. In fact, several experimental studies [17, 59, 60] have shown that O_2 (or O) oxidation can produce finally $CO_{(g)}$ in spite of this endothermic process has a high energy barrier around 3–4 eV, arising from the adsorbed O. Although this carbon etching is mainly enhanced by defect sites, at temperatures larger than 1,148 K also occurs in basal plane carbon atoms [59]; HOPG samples at 298–493 K exposed to pulsed hyperthermal beams containing atomic and molecular oxygen yield an important and spatially anisotropic etching [19]. For this reason, we have only made calculations with the proposed microkinetic model up to 1,000 K. Therefore, at higher temperatures, these etching processes and another surface processes should be included, as for instance:

$$O_{(g)} + \text{graphite} \rightarrow CO_{(g)} + \text{graphite (vacant)} \quad (10)$$

$$O_{2(g)} + \text{graphite} \rightarrow CO_{2(g)} + \text{graphite (vacant)} \quad (11)$$

In spite of the fact that this kind of microkinetic models are frequently used to simulate the heterogeneous chemical kinetics of dissociate airflow impinging different kind of surfaces [53, 54], with good agreement in comparison with available experimental data (e.g., total heat flux to the surface, γ coefficients,..), more sophisticated Monte Carlo simulations (e.g., N over silica [55], H over graphite [61]) can also be performed including for instance different types of Eley–Rideal mechanisms or the coverage effect through the time evolution of the system.

4 Conclusions

In this work, we have made a periodic DFT study (GGA/RPBE) on the main elementary heterogeneous processes involving atomic and molecular oxygen over a graphite (0001) surface to present a comprehensive view on its reactivity.

DFT calculations on bulk graphite (e.g., lattice parameters, cohesive energy, isotropic bulk modulus, …) and on O_2 molecule show a quite good agreement with experimental data. The use of one or two layers for the slab model of graphite in the study of the elementary processes seems to be equivalent. The introduction of slab relaxation is relevant for both adsorption energies and the different energy barriers.

Atomic adsorption is an activated process, whose energy barrier decreases for lower coverages and under slab relaxation. The O adsorption is mainly produced on C–C bridge sites with a considerable puckering of these carbons. This epoxide-like (COC) ring structure has also been observed in earlier theoretical and experimental studies on graphene and graphite oxides.

Atomic diffusion between bridge sites is also an activated process, with lower energy barriers at low coverages but with higher values when slab relaxation is allowed, due to the larger O_{ad} stabilization.

Atomic recombination processes via ER and LH mechanisms are also activated processes although their energy barriers decrease with coverage increment, especially for ER reaction, which will dominate the atomic recombination reaction from low to high temperatures.

We have proposed a microkinetic model with 6 elementary steps, which confirms the very small contribution of the LH process and predicts a very low atomic coverage (<0. 5%), which along with the small rate constants originates very low atomic recombination coefficients (γ_O). At low temperatures, adsorption and ER reaction are the most important processes with similar contributions, while at high temperatures this occurs for adsorption and desorption processes although in this case their rates are compensated. The increase in O partial pressure augments γ_O while the presence of molecular oxygen has no consequences. Temperature raise enhances γ_O values until reaching a temperature where the desorption becomes very important, hence diminishing γ_O.

We may expect that the inclusion of lattice relaxations could be less important for O/O_2 over graphite than for another solid surfaces because the gas/solid interactions are much lower. Nevertheless, we are working in the construction of interpolated PESs for both O/graphite and O_2/graphite systems to include properly the solid vibrations into next dynamical studies, which will reveal clearly this phonon effect.

Acknowledgments We are grateful to the Spanish Ministry of Science and Innovation (Project CTQ2009-07647) and to the Autonomous Government of Catalonia (Project 2009SGR1041) for their financial support.

References

1. Ngo T, Snyder EJ, Tong WM, Williams RS, Anderson MS (1994) Surf Sci Lett 314:L817
2. Capitelli M (ed) (1996) Molecular physics and hypersonic flows, NATO ASI Series C, vol 482. Kluwer Academic Publishers, Dordrecht
3. Lamoen D, Persson BNJ (1998) J Chem Phys 108:3332
4. Sorescu DC, Jordan KD, Avouris P (2001) J Phys Chem B 105:11227
5. Incze A, Pasturel A, Chatillon C (2001) App Surf Sci 177:226
6. Incze A, Pasturel A, Chatillon C (2003) Surf Sci 537:55
7. Xu Y, Li J (2004) Chem Phys Lett 400:406
8. Ito J, Nakamura J, Natori A (2008) J App Phys 103:113712
9. Xu Z, Xue K (2010) Nanotech 21:045704
10. Zhu XY, Lee SM, Lee YH, Frauenheim T (2000) Phys Rev Lett 85:2757
11. Walch SP (2003) Chem Phys Lett 374:501

12. Ulbricht H, Zacharia R, Cindir N, Hertel T (2006) Carbon 44:2931
13. Tkatchenko A, Scheffler M (2009) Phys Rev Lett 102:073005
14. Ulbricht H, Moos G, Hertel T (2002) Phys Rev B 66:075404
15. Ulbricht H, Moos G, Hertel T (2003) Surf Sci 532–535:852
16. Barber M, Evans EL, Thomas JM (1973) Chem Phys Lett 18:423
17. Kelemen SR, Freund H (1985) Carbon 23:619
18. Kinoshita H, Umeno M, Tagawa M, Ohmae N (1999) Surf Sci 440:49
19. Nicholson KT, Minton TK, Sibener SJ (2005) J Phys Chem B 109:8476
20. Kresse G, Hafner J (1993) Phys Rev B 47:558
21. Kresse G, Hafner J (1994) Phys Rev B 49:14251
22. Kresse G, Furthmüller J (1996) Comput Mater Sci 6:15
23. Kresse G, Furthmüller J (1996) Phys Rev B 54:11169
24. Hammer B, Hansen LB, Nørskov JK (1999) Phys Rev B 59:7413
25. Perdew JP, Burke K, Ernzerhof M (1996) Phys Rev Lett 77:3865
26. Perdew JP, Burke K, Ernzerhof M (1997) Phys Rev Lett 78:1396
27. Perdew P, Chevary JA, Vosko SH, Jackson KA, Pederson MR, Singh DJ, Fiolhais C (1992) Phys Rev B 46:6671
28. Perdew P, Chevary JA, Vosko SH, Jackson KA, Pederson MR, Singh DJ, Fiolhais C (1993) Phys Rev B 48:4978
29. Blöchl PE (1994) Phys Rev B 50:17593
30. Kresse G, Joubert D (1999) Phys Rev B 59:1758
31. Monkhorst HJ, Pack JD (1976) Phys Rev B 13:5188
32. Henkelman G, Uberuga BP, Jónsson H (2000) J Chem Phys 113:9901–9978
33. Henkelman G, Jóhannesson G, Jónsson H (2000) In: Schwartz SD (ed) Theoretical methods in condensed matter. Kluwer Academic Publishers, Seattle
34. Huber KP, Herzberg G (1979) Molecular spectra and molecular structure, vol. IV, constants of diatomic molecules. Van Nostrand Reinhold, New York
35. Laidler KJ (1987) Chemical kinetics. Harper & Row, New York
36. Wyckoff RWG (1963) Crystal structures. Interscience Publishers, New York
37. Hasegawa M, Nishidate K (2004) Phys Rev B 70:205431
38. Chase MW Jr (1998) NIST-JANAF themochemical tables, fourth Edition, J Phys Chem Ref Data, Monograph 9, American Institute of Physics, New York
39. Birch F (1947) Phys Rev 71:809
40. Gauster WB, Fritz IJ (1974) J App Phys 45:3309
41. Blackslee OL, Proctor DG, Seldin EJ, Spence GB, Weng T (1970) J App Phys 41:3373
42. Jansen HJF, Freeman AJ (1987) Phys Rev B 35:8207
43. Kim E, Chen C (2004) Phys Lett A 326:442
44. Lerf A, He H, Forster M, Klinowski J (1998) J Phys Chem B 102:4477
45. Szabo T, Berkesi O, Forgó P, Josepovits K, Sanakis Y, Petridis D, Dékány I (2006) Chem Mater 18:2740
46. Paci JT, Belytschko T, Schatz GC (2007) J Phys Chem C 111:18099
47. Casolo S, Løvvik OM, Martinazzo R, Tantardini GF (2009) J Chem Phys 130:054704
48. Sha X, Jackson B (2002) Surf Sci 496:318
49. Arasa C, Gamallo P, Sayós R (2005) J Phys Chem B 109:14954
50. Gamallo P, Sayós (2007) Phys Chem Chem Phys 9:5112
51. Arasa C, Morón V, Busnengo HF, Sayós R (2009) Surf Sci 603:2742
52. Kovalev VL, Kolesnikov AF (2005) Fluid Dyn 40:669
53. Barbato M, Reggiani S, Bruno C, Muylaert J (2000) J Therm Heat Trans 14:412
54. Guerra V (2007) IEEE Trans Plasma Sci 35:1397
55. Guerra V, Loureiro J (2004) Plasma Sour Sci Tech 13:85
56. Balat-Pichelin M, Bedra L, Gerasimova O, Boubert P (2007) Chem Phys 340:217
57. Bedra L, Balat-Pichelin M (2005) Aero Sci Tech 9:318
58. Savvatimskiy AI (2005) Carbon 43:1115
59. Hahn JR (2005) Carbon 43:1506
60. Cen P, Yang RT (1984) Carbon 22:186
61. Cuppen HM, Hornekaer L (2008) J Chem Phys 128:174707